Proceedings of the 21st ICSMGE, Vienna, Austria, 14 – 19 June 2026. Pistrol, Adam & Schweiger (eds.)
Published by: ÖGG, Austrian Society for Geomechanics, Salzburg, Austria, ISBN 978-3-9503898-4-5
https://doi.org/10.53243/ICSMGE2026-1338

Three-dimensional beam-plate finite element method and resilient retaining structures design in deep excavations

Xuesong Cheng, Chenkai Li, Gang Zheng, Qinghan Li
Dept. of Civil Engineering, Tianjin University, Tianjin, China

Fan Yi
China Institute of Water Resources and Hydropower Research, Beijing, China, yifan@iwhr.com

Haibin Yang, Jing Zhao
China Railway Construction (Tianjin) Rail Transit Investment Development Co., Ltd., Tianjin, China

ABSTRACT: Designing resilient retaining structures is crucial in excavation engineering, particularly for projects in urban areas where a higher resistance to progressive collapse is required. To address this, this study proposes a rapid three-dimensional excavation design tool, the beam-plate finite element method (BPFEM), for designing retaining structures in braced-excavations. The reliability of the proposed method is validated through comparisons with results from commercial software and field measurements. The proposed method is suitable for modeling braced retaining structures in three-dimensional space. Furthermore, its fast computation speed enables the application of alternative path analysis in three dimensions, where individual structural components are removed sequentially to assess the potential for progressive failure. In robust retaining systems, each structural component exhibits high safety, ensuring that the removal of any single component does not lead to subsequent failures. Case studies of braced excavations demonstrate that the failure of struts located at corners or near the bottom of the excavation is more likely to trigger subsequent structural failures, potentially leading to the progressive collapse. These findings highlight the critical importance of giving special attention to these areas during excavation design and construction.

KEYWORDS: braced-excavation engineering, beam-plate finite element method, progressive failure, resilient design.

1 INTRODUCTION

1.1 *Resilient design methods*

Research on structural robustness in superstructures has advanced significantly, with robustness indicators now systematically classified across four dimensions: abnormal events, local damage, non-proportional failure, and failure consequences (Lv, 2011). Recent work further proposes resilient approaches to arrest collapse propagation following initial failures (Makoond, 2024). The evolution of evaluation methodologies has progressed toward multi-scale and multi-indicator frameworks (Ghosn & Moses, 1998) as well as the full probability analysis (Felipe, 2018), enabled by computational advances that simultaneously model various failure modes and complex environmental interactions. This integrated approach enhances assessment accuracy while optimizing structural designs for improved disaster resilience and safety.

However, there is still a lack of systematic method for resilient design in geotechnical engineering. Current reliability analysis in excavation engineering adopted safety factor served as the performance function, where the random variables typically account for soil parameter heterogeneity and retaining component strength (Liu, 1998; Zhao, 2012; Zhu, 2010). From the excavation redundancy perspective, Zheng (2011) first introduced the concept to geotechnical systems. Subsequent studies advanced risk quantification through load transfer coefficients and robustness coefficients (Yi, 2023), targeting structural failure potential.

1.2 *Shortcomings of current 3D simulation methods*

The current commonly used three-dimensional finite element numerical simulation methods, while accurate, are time-consuming, making them impractical for real-time evaluation of excavation resilience during construction and in response to emergencies.

The prevalent commercial engineering design softwares, such as the *BSC3D* and *F-SPW* in China, are not capable of analyzing the redundancy of structures. The *BSC3D* software performs coordinated computational analysis: horizontal strut deformations are calculated under applied loads, then iteratively transferred to vertical pile sections for axial force back-calculation until convergence. Since the calculation is performed only on a single 2D cross-section at a time, the computational speed is relatively fast. However, this sequential single-cross-section analysis fails to capture the integrated behavior of horizontally continuous structures like diaphragm walls. Besides, F-SPW addresses this limitation through fully coupled 3D structural analysis but remains constrained in resilient design applications. It cannot implement element removal approach for redundancy assessment (Cimellaro, 2010) due to its closed-source characteristic.

To enhance computational efficiency and facilitate practical application in resilient excavation design, this paper introduces the three-dimensional beam-plate finite element method (BPFEM).

2 THEORY OF BPFEM

BPFEM serves as a simplified calculation method, aiming to enhance the calculation efficiency. Hence, there are some simulation assumptions should be mentioned before the theory introduction:

1. The soil is equivalent to line load outward the excavation and linear springs inward.
2. Owing to the small deformation assumption, the soil and structures are considered as linear elastic model.
3. As a reason of the equivalent calculation for soil pressure, the pressure variation caused by soil arch effect is not considered, which limits this software to analyze before initial failure.

The calculation flowchart of the BPFEM is depicted in Figure 3, including pre-processing, analysis and the post-processing. In this section, the calculation theory of BPFEM is specified.

2.1 *Pre-processing*

The proposed simulation method is based on the open-source structural analysis software *PyNite*. The novelty of this study

lies in the development of a step-by-step deep excavation calculation module and a post-processing module for visualization. The core simulation process relies on *PyNite*'s well-established finite element analysis algorithms. Therefore, fundamental principles of finite element analysis are not detailed in this section. Additionally, the computational framework for excavation retaining structures is implemented based on the Chinese deep excavation design code (JGJ120-2012), using the following governing equations:

$$M=EI\rho=-EI\frac{d^2x}{dz^2} \tag{1}$$

$$Q=\frac{dM}{dz}=-EI\frac{d^3x}{dz^3} \tag{2}$$

$$-\frac{dQ}{dz}=EI\frac{d^4x}{dz^4}=e_{ak}b_s-k_pb_0x \tag{3}$$

$$Q_{Z_{si}}=-EI\frac{d^3x}{dz^3}\Big/_{Z=Z_{si}}=-K_{si}b_s\left(x^m_{Z_{si}}-x^{m-1}_{Z_{si}}\right)-T_{0i} \tag{4}$$

$$M_{zL}=-EI\frac{d^2x}{dz^2}\Big/_{Z=Z_L}=-K_\theta\frac{dx}{dz}\Big/_{Z=Z_L} \tag{5}$$

Where M is the bending moment of the retaining pile; E is the Young's modulus of the retaining pile; I is the inertia of the retaining pile; ρ is the curvature of the retaining pile; z is depth; x is the horizontal deformation; Q is the shearing force in the retaining pile; e_{ak} is the earth pressure in the active zone; k_p is the soil spring stiffness in the passive zone, where $k_p = m \cdot z$, and m is the coefficient of subgrade reaction; b_s is the calculating width in the active zone, which equals the spacing between retaining piles; b_0 is the calculating width of the soil in the passive zone, where $b_0=0.9(1.5d+0.5)$, and d is the diameter of the retaining pile; z_{si} is the depth of the i th level of strut; K_{si} is the horizontal stiffness of the strut in unit width; x^m_{Zsi} is the horizontal deformation in case m at the elevation of the i th level of strut; T_{0i} is the prestressed force in the strut; z_L is the depth of the pile toe; M_{ZL} is the bending moment of the pile toe; K_θ is the bending stiffness of the pile toe.

In the simulation, the earth pressure in the active zone is calculated by Rankine's earth pressure theory, while the soil in the passive zone was equated to passive springs followed by the equation below.

$$m=\frac{1}{\Delta}(0.2\varphi^2-\varphi+c) \tag{6}$$

Where Δ is the estimated bottom displacement of the excavation; φ is the soil friction; c is the soil cohesion.

Thus, the soil parameters play an essential role in simulation results. Specifically, the soil friction and cohesion account for the pressure value and the spring stiffness. As illustrated in Figure 1, for each grid point in the diaphragm wall, the algorithm automatically identifies adjacent grid points and calculates the area of the rectangular region formed by their envelope. The equivalent supporting area of each spring is determined by dividing this area by 4, and the spring stiffness is computed by multiplying the stiffness per unit area by the supporting area.

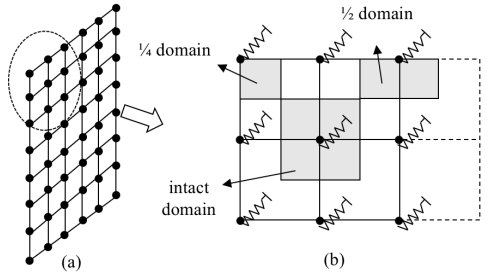

Figure 1. Schematic of soil spring stiffness calculation.

2.2 *Step-by-step excavation calculation*

After inputting the parameters, the earth pressure in the active zone and soil springs in the passive zone are applied. The primary FEM calculation process is integrated into *PyNite*, as shown in Figure 3. Since the core calculations in *PyNite* are based on a stable equilibrium approach and do not support incremental calculations, additional procedures have been implemented to simulate step-by-step excavation. As illustrated in Figure 2, a displacement load module has been developed to perform incremental displacement calculations, accounting for both excavation and strut installation. Initially, it is assumed that the piles are undeformed before excavation, with earth pressure applied in the active zone and soil springs in the passive zone. Excavation is simulated by progressively removing soil springs in the passive zone. After excavating the first layer of soil, the displacement at the first layer of struts, denoted as Δ_{p1}, is monitored and incorporated before the second excavation step. Similarly, after the second excavation step, the displacement at the second layer of struts, Δp_2, is monitored. Before removing the third layer of soil springs, the displacements Δ_{p1} and Δ_{p2} are accounted for, along with the installation of the second layer of strut springs. These preset displacements can account for the displacement of the diaphragm wall at the location of struts before installing the struts.

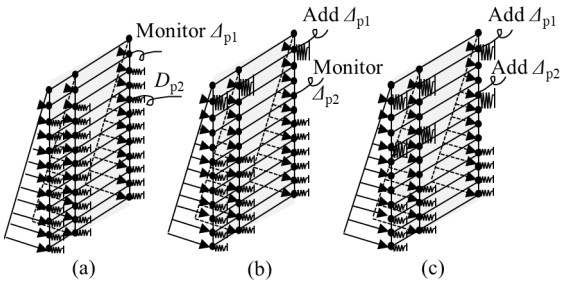

Figure 2. Excavation simulation process: (a) First step of excavation; (b) Installing the first layer of struts and second step of excavation; (c) Installing the second layer of struts and third step of excavation.

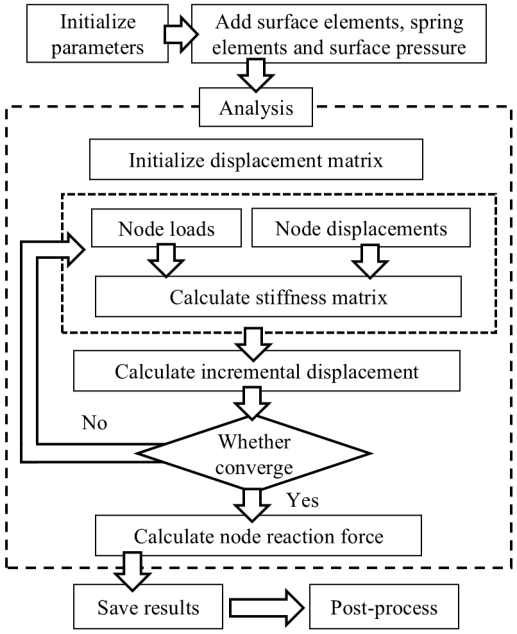

Figure 3. The calculation flowchart of BPFEM.

3 VERIFICATION OF BPFEM

To validate the algorithm for deep excavation problems, this simulation method has been applied to case models in this study, enabling a resilience evaluation.

3.1 *Comparison with FRWS*

In this section, the validity of BPFEM was validated by comparing the BPFEM simulation results with those obtained from the commercial engineering design software *FRWS9.0*, based on two excavation cases. Besides, the progressive failure process was also simulated, pointing out the limitations of BPFEM.

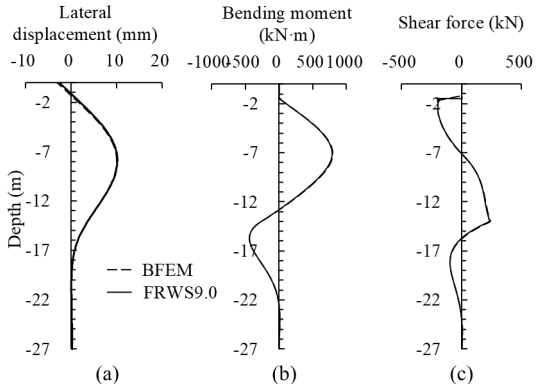

Figure 4. Comparison between the BFEM method and the commercial software FRWS 9.0: (a) Lateral displacement of the diaphragm wall; (b) Bending moment of the diaphragm wall; (c) Shearing force of the diaphragm wall.

Verification of beam finite element method (BFEM)

A propped pile-retaining excavation in Hangzhou, China was selected to verify the BFEM, since the pile components in this case can be simulated as beam elements and the struts as spring elements. Hence, a two-dimension BFEM model and a FRWS model were established, using the same parameters (soil and structure). And the simulation results were compared in Figure 4, figuring excellent curve fitting in terms of lateral displacement, bending moment and the shear force. This alignment verifys the validity of the proposed BFEM algorithm.

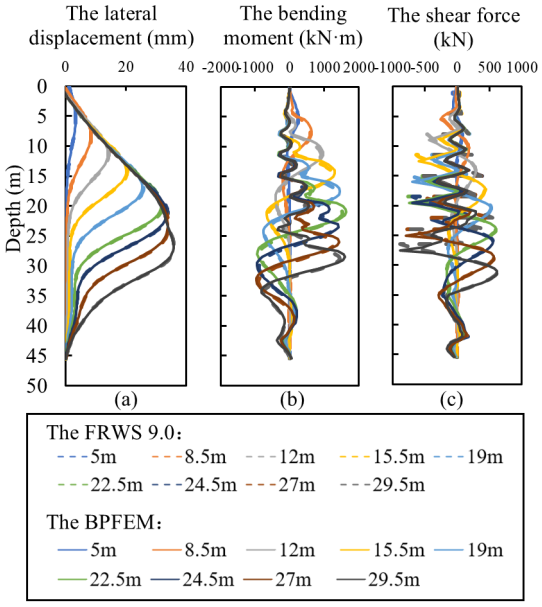

Figure 5. Comparison between the PFEM method and the commercial software FRWS 9.0: (a) Lateral displacement of the diaphragm wall; (b) Bending moment of the diaphragm wall; (c) Shearing force of the diaphragm wall.

Verification of plate finite element method (PFEM)

The PFEM was verified through a strutted wall-retaining excavation case in Singapore (COI, 2004). In this case, the diaphragm wall was simulated as plate element and the struts as spring elements. The step-by-step simulation approach provided displacement and internal force calculations that align well with the *FRWS9.0* results, demonstrating excellent curve fitting in terms of lateral displacement and bending moment (Figure 5). This agreement supports the validity of the proposed PFEM algorithm.

3.2 *Progressive failure*

Compared to the *FRWS9.0*, the BPFEM can simulate the load redistribution after local failure, which enables it to analyze the redundancy of retaining structure. For the analysis, a straightforward approach is removing structural elements that exceed their bearing capacity (BS 8110-1: 1997), called element removal approach. In this section, the progressive struts failure was simulated by FDM method and BPFEM. Each strut was labeled based on its layer and horizontal position. For example, $S_{9\text{-}1}$ represents the first strut in the ninth layer.

In the FDM simulation, the $S_{9\text{-}1}$ strut was removed (e.g., marked by red crosses in Figure 6). The sequence of strut failures is illustrated in Figure 6(a). From Figure 6(a), it is evident that the failure of $S_{9\text{-}1}$ triggered the failure of the adjacent $S_{9\text{-}2}$ strut. Meanwhile, the axial force in the $S_{8\text{-}1}$ strut increased sharply, but it did not fail at this stage. Following the local failure of $S_{9\text{-}1}$, the progressive failure mainly spread horizontally due to the low safety factor of the ninth layer of struts.

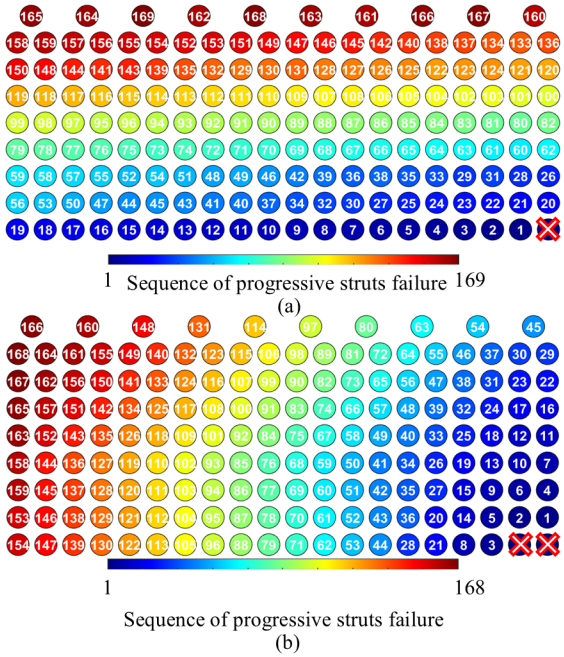

Figure 6. Sequence of progressive strut failure: (a) FDM results; (b) BPFEM results.

However, the BPFEM simulation, as shown in Figure 6(b), required the failure of at least two struts to initiate progressive collapse. This indicates that FDM provides a more conservative prediction compared to the BPFEM method. The failure propagation pattern differed depending on the strut level. In the sixth to ninth layers, strut failures generally spread horizontally, whereas in the upper layers (first to fifth), failure expanded in a fan-shaped pattern from the lower right corner toward the upper left (Figure 6(b)). This sequence variation, compared to the FDM results, was primarily due to the stepwise calculation method used in BPFEM. In this approach, strut failure was

modeled by removing struts that exceed their bearing capacity at the end of each calculation step. The simulation then proceeded to the next step, iterating until all struts have failed. However, as the BPFEM method employs implicit calculations, it did not capture the precise sequence of strut failures within each step. As a result, multiple struts may fail simultaneously after each step of calculation. Furthermore, the BPFEM method did not account for the soil arching effect, leading to reduced soil pressure around failed struts and influencing adjacent areas. For these limitations, the BPFEM can only be used as safety evaluation before the occurrence of local failure.

4 RESILIENT EXCAVATION DESIGN

Based on the excavation case in Section 3.1, a three dimensional (3D) BPFEM model was established in this section, analyzing the robustness of the retaining system using element removal approach. Additionally, a systematic resilient design method is proposed based on BPFEM.

4.1 *The BPFEM model*

To enhance the reality of the model, the struts were simulated as the beam elements, different from the spring elements in section 3.1. Furthermore, four monitored pile were set in the model (the red circle in Figure 7(a)), monitoring their lateral displacements and the internal forces.

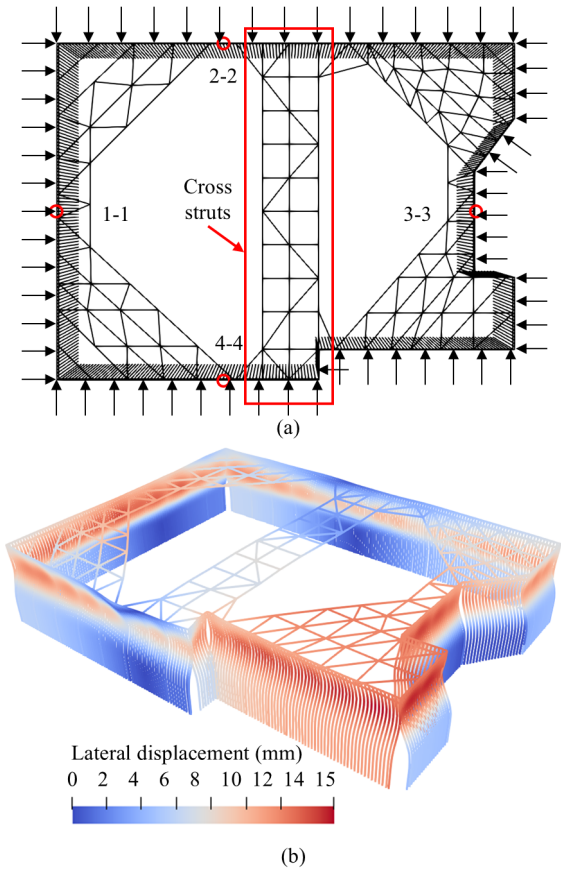

Figure 7. The 3D-BPFEM model: (a) model schematic; (b) the overall deformation contour.

The overall deformation contour of the 3D model is shown in Figure 7(b), and the comparison between 2D and 3D models is presented in Figure 8. From these figures, it can be observed that the maximum bending moment and shear force in the 2D model are higher than those in the 3D model. Regarding pile displacement, the maximum displacements of the retaining piles in sections 1-1 and 3-3 are greater than those in the 2D model, while the maximum displacements in sections 2-2 and 4-4 are smaller than in the 2D model. The main reason for this difference lies in the support configuration. In sections 2-2 and 4-4, the retaining piles are located where a opposite struts is present. This results in a higher supporting stiffness, which reduces the pile displacement. In contrast, in sections 1-1 and 3-3, the retaining piles are located within the area of corner sturts. Since the stiffness of corner struts is relatively low, these piles experience larger lateral displacements at the pile head. Besides, in this BPFEM simulation, the 3D model shows greater deformation compared to the 2D model, which contrasts with general finite element analysis practices. As for the reason, in real 3D excavation models, the stiffness at the corner is higher and the soil pressure is lower due to three-dimensional space effect, compared to the 2D plane strain assumption. In the current 3D-BPFEM model, however, the soil pressure is still modeled in a simplified manner, which neglects the 3D space effect. As a result, the actual reduction in soil pressure and the increased corner stiffness are not captured, leading to higher displacements in the 3D model than expected.

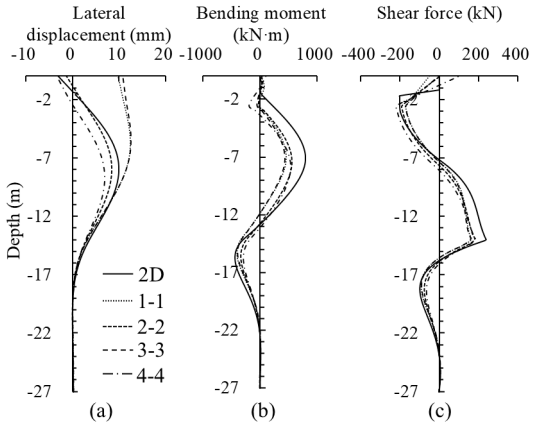

Figure 8. Comparison between the 2D-BFEM method and the 2D-BFEM method: (a) Lateral displacement of the diaphragm wall; (b) Bending moment of the diaphragm wall; (c) Shearing force of the diaphragm wall.

4.2 *Robustness analysis*

Robustness refers to the ability of tolerating perturbations that might affect the function of the system. As mentioned in Section 3.2, a straightforward method to analyze the redundancy of retaining structure is element removal approach. During the removal of struts, the released loads cause redistribution of internal forces within the retaining structure. It is evident that different systems exhibit varying capacities to resist these loads, which reflects their resilience against potential failure. In order to quantitatively evaluate it, this section proposes the robustness coefficient (*RC*, referred to Equation (7)) to assess the internal force redistribution characteristics and the capacity to resist potential failure of the retaining system.

$$RC = min\left(\frac{\hat{N}-N}{\hat{N}}\right) \tag{7}$$

Where N is the internal force of component, $\hat{N}$ is the bearing capacity of the component. When *RC* exceeds 0, the system remains safe. Otherwise, the component failure will occur.

Regarding the limitation of BPFEM mentioned in Section 3.2, the robustness of the overall propped system is evaluated from the perspective of excavation design in this section, without considering the progressive failure.

As shown in Figure 9, the *RC* of strut member is illustrated after one-strut removal. The minimum *RC* (overall *RC*) is shown in Figure 9, representing the robustness of excavation after the strut removal. Before the strut was removed, the cross struts in the system bear greater axial forces, indicating better

support performance. Besides, these opposite struts exert a stronger rotational constraint at the pile head, causing larger bending moments at the corresponding nodes. Hence, the axial force and bending moment robustness near the location of the opposite struts is relatively low. After the strut was removed, due to the effect of the convex corner in the southern central part of the excavation, and the removal of the corner strut, the stiffness in the central region of the excavation suddenly decreased. This caused the convex corner to deform inward, resulting in a significant reduction in the *RC* of the strut marked by the red circle in Figure 9, from 2.0 to 1.6, making it the most vulnerable strut in the system. In contrast, the robustness of the bending moments remains unchanged, and the minimum *RC* of the excavation still remains at 0.1. From the above analysis, it can be concluded that the convex corners in the excavation have a notably adverse effect on its overall safety. Therefore, in excavation design, such convex corners should be avoided as much as possible. When it is inevitable, necessary reinforcement should be implemented at these critical corner locations.

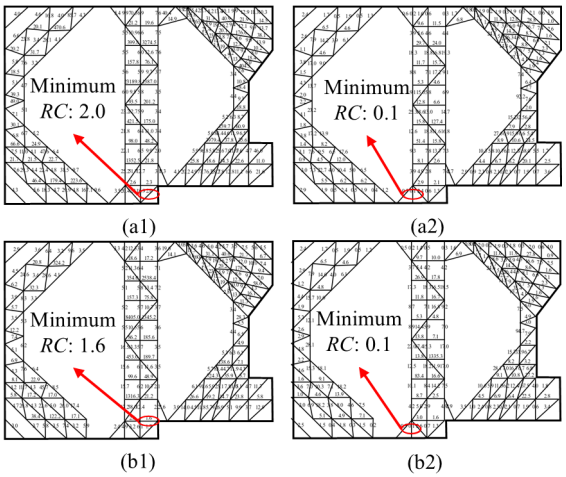

Figure 9. The *RC* of retaining system: (a1) axial force before removal; (a2) axial force after removal; (b1) bending moment before removal; (b2) bending moment after removal.

The robustness coefficient (*RC*) varies with the removal of different struts. To evaluate excavation robustness, we calculate the *RC* after each individual strut removal, with the minimum *RC* value representing the overall *RC*. As illustrated in Figure 10(a1) and (a2), strut members are sequentially removed in simulations, and the axial force and bending moment *RC* are computed for each scenario. Shear force *RC*, being consistently high across removals, is omitted for clarity and conciseness. Each strut in the figures is annotated with the overall *RC* value following its removal, enabling visual identification of critical members. Struts associated with the lowest robustness values indicate where failure would most significantly compromise structural stability.

It is evident from the figures that the central cross struts are more prone to induce progressive failure after removal. This is primarily because the central region is subjected to higher internal forces, and the presence of the convex corner in this area exacerbates the stress concentration. Specifically, as shown in Figure 10(a2), the removal of any single strut member located in the southern convex corner region results in an overall robustness less than 0, which indicates that progressive failure is inevitable in this scenario. In contrast, removing a strut member located on the opposite struts but away from the convex corner does not necessarily lead to progressive failure. This observation highlights that the convex corner region of the excavation exhibits significantly lower robustness, and every member in this area can be considered a critical component. Therefore, during the excavation construction, attention and protection should be given to the convex corner region to prevent progressive failure caused by the failure of any single member in this area. It is also worth noting that, although the eastern side of the excavation also contains a convex corner, the overall *RC* in this region is higher compared to the southern side. This is due to lower stress levels and the presence of a denser arrangement of corner struts in this region.

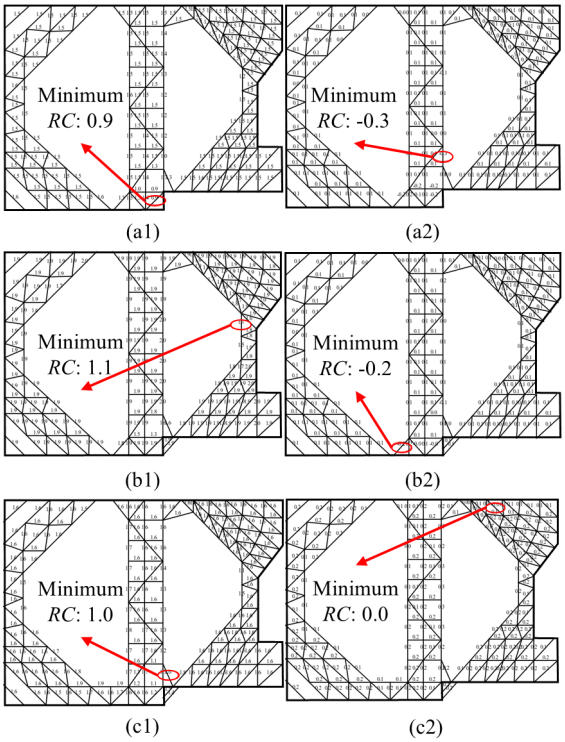

Figure 10. The overall *RC* of retaining system: (a1) axial force *RC* in original design; (a2) bending moment *RC* in original design; (b1) axial force *RC* in strengthened Case 1; (b2) bending moment *RC* in strengthened Case 1; (c1) axial force *RC* in strengthened Case 2; (c2) bending moment *RC* in strengthened Case 2.

4.3 *Resilient design measures*

From the previous section, it is understood that the removal of strut members at the convex corner of the excavation results in the overall robustness of the retaining system dropping below 0, which may lead to progressive failure. To address this issue, this section presents a targeted improvement to the strut system, aiming to enhance the robustness of the entire retaining system.

As shown in Figure 10(b1) and (b2), two concrete corner struts are added at the active zone of the capping beam in the convex corner region, enhancing the stiffness of the convex corner and increasing the load transfer paths. From the figures, it can be observed that, compared with Figure 10(a1) and (a2), with the additional corner struts, the strut member with the lowest robustness in the system has shifted from the opposite strut to the eastern side of the excavation. Moreover, as presented in Table 1, the axial force robustness of the system has been improved from 0.9 to 1.1. However, for the bending moment robustness, although it has increased from -0.3 to -0.2, it is still less than 1. This indicates that simply strengthening corner struts to the active zone of the convex corner is insufficient to fully prevent the potential failure risk of the excavation.

The insufficient robustness in the southern convex corner region is attributed to the mismatch in struts stiffness between the southern side and the southwest side. Specifically, the

southern side is supported by opposite struts, while the southwest side is supported by corner struts, resulting in incompatible stiffness and causing the strut members to experience significantly higher bending moments. Therefore, it is necessary to connect the corner struts and opposite struts, ensuring the compatibility of deformation of the structures.

As shown in Figure 10(c1) and (c2), in addition to adding two corner braces to reinforce the active zone of the convex corner, two horizontal tie bars are set to connect the retaining structures between the southern and southwest structures. From the figures, it can be observed that after implementing this measure, although the minimum robustness for axial force still occurs in the convex corner region, its value is 1.0, indicating that the system now has a safety margin. For bending moment robustness, it has improved from -0.3 to 0.0, and the location of the minimum robustness is no longer in the southern convex corner. Although the minimum robustness value is still close to 0, this suggests that the safety redundancy is low, but collapse is not imminent. To further enhance the robustness of the retaining system, it is advisable to specifically increase the load capacity of those members with robustness values near 0, thereby reducing the probability of initial failure.

Table 1. The robustness of retaining system.

Cases	Axial force	Bending moment	Shear force
Original design	0.9	-0.3	0.5
Reinforcing the convex corner	1.1	-0.2	0.4
Reinforcing the convex corner + tie bars	1.0	0.0	0.4

5 CONCLUSIONS

This study proposed an effient simulation method BPFEM, efficient to evaluating the robustness of excavation system. Additionally, specific resilient design method was proposed based on BPFEM, exhibiting an example to show the efficiency for resilient excavation design. The key findings are as follows:

1. The BPFEM provides a rapid evaluation of excavation robustness during construction using the component removal approach.
2. Due to simplifications in modeling earth pressure and passive soil springs, it has limitations in capturing the detailed progressive collapse process.
3. The BPFEM is effective for quick safety assessments. The current version of this method is only suited for analyzing the robustness of excavation before failure.
4. The robustness of excavation can be quantified using the robustness coefficient (*RC*) to separately assess the internal force redistribution characteristics and the capacity to resist progressive failure of the retaining system.

6 ACKNOWLEDGEMENTS

This work was supported by the National Key Research and Development Program of China (No. 2023YFC3009300), the Tianjin Science Foundation for Distinguished Young Scientists of China (No. 24JCJQJC00170), the China Postdoctoral Science Foundation under Grant Number (No.2025M773243), and the Postdoctoral Fellowship Program of CPSF under Grant Number (No. GZC20252133). Their support is gratefully acknowledged.

7 REFERENCES

British Standard Institute, 1997. *BS 8110-1: 1997 Structural use of concrete: Part 1: Code of practice for design and construction.* British: BIS.

Cimellaro, G. P., Reinhorn, A. M., Bruneau, M. 2010. Framework for analytical quantification of disaster resilience. *Engineering structures* 32(11): 3639-3649.

COI. 2004. *Report of the Committee of Inquiry into the incident at the MRT circle line worksite that led to collapse of Nicoll Highway on 20 April 2004.* Singapore: Ministry of Manpower.

Felipe, T. R. C., Haach, V. G., Beck, A. T.. 2018. Systematic reliability-based approach to progressive collapse. *ASCE-ASME Journal of Risk and Uncertainty in Engineering Systems, Part A: Civil Engineering.* 4(4): 04018039.

Ghosn, M., & Moses, F. 1998. Redundancy in highway bridge superstructures. *Journal of Structural Engineering* 124(5): 525-533.

Liu, G. B., Shen, J. M., Hou, X. Y.. 1998. The reliability analysis of retaining system in deep excavation. *Journal of Tongji University (Natural Science)* (03): 260-264.

Lv, D. G., Song, P. Y., Cui, S. S., and Wang, M. X.. 2011. Structural robustness and its assessment indicators. *Journal of Building Structures (China)* 32 (11): 44-54.

Makoond, N., Setiawan, A., Buitrago, M. et al. 2024. Arresting failure propagation in buildings through collapse isolation. *Nature* 629, 592-596.

Ministry of Housing and Urban-Rural Development of PRC. 2012. *JGJ120-2012 Technical Specification for Retaining and Protection of Building Foundation Excavations*. China Architecture & Building Press.

Murtha-Smith E.. 1988. Alternate path analysis of space trusses for progressive collapse. *Journal of Structural Engineering* 114(9):1978–1999.

Yi, F., Su, J., Zheng, G., Cheng, X., Pei, H., Liu, X. and Jia, J. 2023. Progressive collapse analysis and robustness evaluation of a propped excavation failed due to inappropriate strut removal. *Acta Geotech*. 18: 6775-6801.

Zhao, Y. L.. Reliability analysis of stability and deformation in deep foundation pit. Harbin Engineering University. [Online] Available at: http://lib.hrbeu.edu.cn/ [Accessed 9th March 2012].

Zheng, G., Cheng, X. S., Diao, Y., and Wang, H. X.. 2011. Concept and Design Methodology of Redundancy in Braced Excavation and Case Histories. *Geotechnical Engineering Journal of the SEAGS & AGSSEA* 42(3): 13-21.

Zheng, G., Cheng, X. S., Zhang Y.. 2014. Simulation of progressive collapse and redundancy of ring-beam supporting structures of excavations. *Chinese Journal of Geotechnical Engineering* 36(01): 105-117.

Zhu, J. F., Chen, C. F., Xu, R. Q.. 2010. An optimization method of reliability analysis of foundation pit reinforced with soil nailing. *Rock and Soil Mechanics (China)* 31(07): 2336-2341.